Topological bifurcations in a model society of reasonable contrarians

Franco Bagnoli*
Dipartimento di Fisica e Astronomia, Università di Firenze, Via G. Sansone 1, 50017 Sesto Fiorentino (FI), Italy and INFN, sez. Firenze, Italy

Raúl Rechtman†
Instituto de Energías Renovables, Universidad Nacional Autónoma de México, Apdo. Postal 34, 62580 Temixco Mor., Mexico
(Received 20 August 2013; published 10 December 2013)

People are often divided into conformists and contrarians, the former tending to align to the majority opinion in their neighborhood and the latter tending to disagree with that majority. In practice, however, the contrarian tendency is rarely followed when there is an overwhelming majority with a given opinion, which denotes a social norm. Such reasonable contrarian behavior is often considered a mark of independent thought and can be a useful strategy in financial markets. We present the opinion dynamics of a society of reasonable contrarian agents. The model is a cellular automaton of Ising type, with antiferromagnetic pair interactions modeling contrarianism and plaquette terms modeling social norms. We introduce the entropy of the collective variable as a way of comparing deterministic (mean-field) and probabilistic (simulations) bifurcation diagrams. In the mean-field approximation the model exhibits bifurcations and a chaotic phase, interpreted as coherent oscillations of the whole society. However, in a one-dimensional spatial arrangement one observes incoherent oscillations and a constant average. In simulations on Watts-Strogatz networks with a small-world effect the mean-field behavior is recovered, with a bifurcation diagram that resembles the mean-field one but where the rewiring probability is used as the control parameter. Similar bifurcation diagrams are found for scale-free networks, and we are able to compute an effective connectivity for such networks.

DOI: 10.1103/PhysRevE.88.062914 PACS number(s): 05.45.Ac, 05.50.+q, 64.60.aq, 64.60.Ht

I. INTRODUCTION

The use of statistical physics methods [1] in the study of social and economic systems is based on the fact that there are global quantities that are not influenced by individual preferences or opinions as in the study of election systems [2] and social networks [3]. Opinion dynamics has been investigated from the point of view of phase transitions [4] and evolutionary dynamics [5]. In the first case, one is interested in the asymptotic behavior of a global quantity when one or more parameters change.

We can think of the many models inspired by the Ising or Potts dynamics where the possible opinions and the affinity between individuals are mapped to spin variables and to spin couplings, respectively. The outstanding feature of opinion formation models is the social network that has no counterpart in spin systems since these are in general associated to regular lattices. By changing the strength of the affinity we can find a phase transition showing, for instance, the conditions for the existence of a well-defined majority [6]. Instead of an equilibrium situation, we may also be interested in the geometry of the basins of attraction for irreversible dynamics, like in Deffuant opinion dynamics [7].

Similarly to antiferromagnetic couplings in Ising models, contrarians can have an opinion opposite to the average opinion of the neighboring agents that may act as a disordering field that prevents the formation of a majority. Contrarian agents were first discussed in the field of finance [8] and later in opinion formation models [9]. Contrarian behavior may have an advantage in financial investment. Financial contrarians look for mispriced investments, buying those that appear to be undervalued by the market and selling those that are overpriced. In opinion formation models, contrarians gather the average opinion of their neighbors and choose the opposite one. Contrarians in irreversible opinion dynamics using an annealed approach [10] lead to a behavior similar to that observed in the Galam model [9].

Another important component is the network structure which can be random (quenched or annealed), regular, with long-range connections (Watts and Strogatz small world) [11], or with a scale-free structure [12], and so on. Indeed, the behavior of a spatial social game is strongly influenced by the network structure [13]. These studies can be extended to include variable network connections [14], depending, for instance, on the difference in opinion [15].

In most of these studies the "agents" do not change their strategy: Conformists remain conformists and contrarians remain contrarians. On the other hand, one may be concerned with the emergence of strategies, generally in the framework of game theory [16]. In this case, the strategy may change due to selection (elimination of low-fitness individuals) or imitation of high-fitness ones (which constitutes a sort of metastrategy). One can be interested in the conditions for which contrarian behavior emerges.

In general, in the presence of weak selection [17] it is natural to assume that the imitation takes the form of a growing function of fitness, for instance, the Fermi distribution [18]. This imitation strategy consists in "running a bit ahead of the group," but there may be cases in which this is not the most sensible thing to do. In particular, in minority games [19] (which were introduced as a metaphor of markets) it might be convenient to stay away from the majority, and this can be a reason for which contrarian behaviors emerge.

*franco.bagnoli@unifi.it
†rrs@cie.unam.mx

However, the contrarian behavior has limits. In any society there are "social norms" that are adopted and respected even if in contrast with an agent's immediate advantage, or, alternatively, even if they are costly with respect to a naive behavior. Indeed, the social pressure towards a widespread social norm is sometimes more powerful than a norm imposed by punishments.

Also in the context of minority games and markets, it might be convenient to follow social norms. When a large majority of agents do the same thing, it is convenient for any agent to follow the majority. The competitive loss in case of common failure is minimum, since it is shared by a large fraction of competitors.

We shall denote as reasonable contrarian the contrarian attitude that does not violate social norms. In other words, a reasonable contrarian disagrees with a marginal majority but agrees if the majority of neighbors is above a certain threshold.

In this paper we are interested in the study of models of a society of reasonable contrarians on different topologies. We show that nontrivial asymptotic states appear, characterized by oscillations and chaotic behavior (in contrast with the simple fixed point asymptotic state of conformists and mixed conformists-contrarians systems).

One of the main motivations of this study is that of exploring the possible behavior of autonomous agents employed in algorithmic trading in an electronic market. Virtually all markets are now electronic [20] and the speed of transaction requires the use of automatic agents (algorithmic trading) [21]. Our study can be considered as an exploration of possible collective effects in a homogeneous automatic market.

The model, presented in Sec. II, simulates a society of N reasonable contrarians that can express one of two opinions, 0 and 1. It is essentially a cellular automaton model [22], which can be seen also as a spin system. At each time step, each agent changes his or her opinion according to a transition probability that takes into account the average opinion of his or her neighbors, that is, the local social pressure, and the adherence to social norms. The neighborhoods are fixed in time (quenched network).

In spin language, the contrarian character corresponds to an antiferromagnetic linear coupling, while social norms can be represented as plaquette terms since they are nonadditive and important when the social pressure is above or below given thresholds.

For a one-dimensional society where the neighborhood of each agent includes its k nearest neighbors, the average opinion fluctuates around the value $1/2$, regardless of the values of the parameters of the transition probability. Simulations of the one-dimensional version of the model show irregular fluctuations at the microscopic level, with short-range correlations [23].

The mean-field approximation of the model for the average opinion is a discrete map which exhibits bifurcation diagrams as the parameters k and J change, as discussed in Sec. III. The diagrams show a period doubling route towards chaos.

In Sec. IV we discuss the model on Watts-Strogatz networks that exhibit the small-world effect [11]. We find a bifurcation diagram as the fraction p of rewired links changes. Since the opinion of agents change probabilistically, we speak of probabilistic bifurcation diagrams.

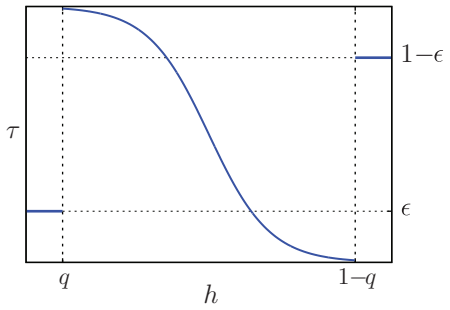

FIG. 1. (Color online) The transition probability $\tau(h)$ given by Eq. (3) with $J=-3$, $k=20$, $q=0.1$, and $\varepsilon=0.2$.

In Sec. V, the reasonable contrarian opinion model is extended to scale-free networks. Again, we observe a probabilistic bifurcation diagram, similar to the previous ones, by varying the coupling J. We are able to obtain a good mapping of the scale-free parameters onto the mean-field approximation with fixed connectivity k.

In order to compare the deterministic and probabilistic bifurcation diagrams, we exploit the entropy η of the average opinion. In the deterministic case, large values of η correspond to positive values of the Lyapunov exponent. In Secs. III, IV, and V we show that η can be used to characterize numerically order and disorder in deterministic and probabilistic bifurcation diagrams. Finally, we present some conclusions.

II. THE MODEL

Each of the N agents has opinion $s_i(t)$ at the discrete time t with $s_i \in \{0,1\}$ and $i=0,\ldots,N-1$. The state of the society is $\boldsymbol{s}=(s_0,\ldots,s_{N-1})$. In the context of cellular automata and discrete magnetic systems, the state at site i is s_i and the spin at site i is $\sigma_i=2s_i-1$, respectively. The average opinion c is given by

$$c=\frac{1}{N}\sum_i s_i. \tag{1}$$

The opinion of agent i evolves in time according to the opinions of his or her neighbors, identified by an adjacency matrix with components $a_{ij}\in\{0,1\}$. If agent j is a neighbor of agent i, $a_{ij}=1$, otherwise $a_{ij}=0$. The adjacency matrix defines the network of interactions and is considered fixed in time. The connectivity k_i of agent i is the size of his or her neighborhood,

$$k_i=\sum_j a_{ij}.$$

The average local opinion or social pressure h_i is defined by

$$h_i=\frac{\sum_j a_{ij}s_j}{k_i}. \tag{2}$$

The opinion of agent i changes in time according to the transition probability $\tau(s_i|h_i)$ that agent i will hold the opinion s_i at time $t+1$ given the local opinion h_i at time t. This

transition probability, shown in Fig. 1, is given by

$$\tau(h) = \begin{cases} \varepsilon & \text{if } h < q, \\ \dfrac{1}{1+\exp(-2J(2h-1))} & \text{if } q \leqslant h \leqslant 1-q, \\ 1-\varepsilon & \text{if } h > 1-q, \end{cases} \quad (3)$$

with $\tau(h) = \tau(1|h)$. The quantity q denotes the threshold for the social norm and ε the probability of being reasonable. With $\varepsilon = 0$ or $q = 0$, $\boldsymbol{s} = (0,\ldots,0)$ and $\boldsymbol{s} = (1,\ldots,1)$ are absorbing states [23]. In the following we set $\varepsilon = 0.2$ and $q = 0.1$ if not otherwise stated. The results are qualitatively independent of ε and q as long as they are small and positive. The transition probability τ has the symmetry

$$\tau(1-h) = 1 - \tau(h). \quad (4)$$

With $J > 0$ and $q < h_i < 1-q$, agent i will likely agree with his or her neighbors, a society of conformists. With $J < 0$ and $q < h_i < 1-q$, agent i will likely disagree with his or her neighbors, a contrarian society. For $0 \leqslant h \leqslant q$ or $1-q \leqslant h \leqslant 1$ agent i will likely agree (if ε is small) with the majority of his or her neighbors, regardless of the value of J.

We might also add an external field H, modeling news and broadcasting media, but in this study we always keep $H = 0$. We are thus modeling a completely uniform society, i.e., we assume that the agent variations in the response to stimuli are quite small. Moreover, we do not include any memory effect, so the dynamics is completely Markovian.

In the language of spin systems, $\tau(h_i)$ is the transition probability of the heat bath dynamics of a parallel Ising model with ferromagnetic, $J > 0$, or antiferromagnetic, $J < 0$, interactions [24]. The behavior of the transition probability in the regions $h < q$ and $h > 1-q$ may be seen as due to a nonlinear plaquette term that modifies the ferroantiferro interaction. If we set $\varepsilon = 0$ and $J = -\infty$, the system becomes deterministic (in magnetic terms, this is the limit of zero temperature).

In one dimension, with $k = 3$, $1/3 < q \leqslant 1/2$, and $\varepsilon = 0$ this model exhibits a nontrivial phase diagram, with two directed-percolation transition lines that meet a first-order transition line in a critical point, belonging to the parity conservation universality class [25]. In this case, we have the stability of the two absorbing states for $J > 0$ (conformist society or ordered phase), while for $J < 0$ (antiferro or contrarian) the absorbing states are unstable and a new, disordered active phase is observed. The model has been studied in the one-dimensional case with larger neighborhood [23]. In this case one observes again the transition from an ordered to an active, microscopically disordered phase but with no coherent oscillations. Indeed, if the system enters a truly disordered configuration, then the local field h is everywhere equal to 0.5 and the transition probabilities τ become insensitive to J and equal to 0.5; see Eq. (3).

III. MEAN-FIELD APPROXIMATION

The simplest mean-field description of the model is given by

$$c' = f(c) = \sum_{w=0}^{k} \binom{k}{w} c^w (1-c)^{k-w} \tau\,(w/k)\,, \quad (5)$$

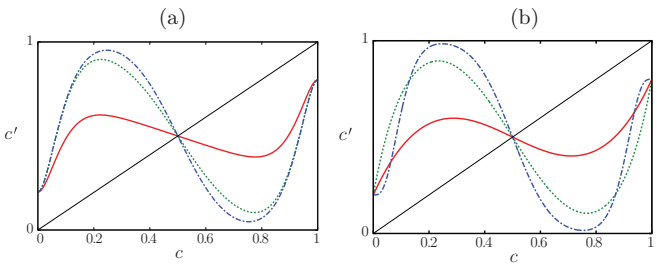

FIG. 2. (Color online) (a) Graphs of the mean-field map, Eq. (5) for different values of J and $k = 20$. From bottom to top for $c < 1/2$, $J = -0.5$ (red, solid line), $J = -3.0$ (green, dotted line), and $J = -6.0$ (blue, dashed-dotted line). (b) Graphs of Eq. (5) for different values of k and $J = -6$. From bottom to top for $c \sim 0.2$, $k = 4$ (red, solid line), $k = 10$ (green, dotted line), and $k = 38$ (blue, dashed-dotted line).

with $c' = c(t+1)$ and $c = c(t)$ [26]. The term in parenthesis on the right-hand side of this expression denotes the w combinations from a set of k elements. In Fig. 2 we show some graphs of f. The map f has the same symmetry property as the transition probabilities τ,

$$f(1-c) = 1 - f(c). \quad (6)$$

The mean-field map, Eq. (5), shows bifurcation diagrams when the parameters J and k change, Figs. 3(a) and 4(a), respectively. Since the mean-field map is deterministic, these bifurcations can be characterized by means of the Lyapunov exponent λ. However, in order to study these diagrams and and those found in the probabilistic models, we use Boltzmann's entropy [27] η of the collective variable c. In the case of deterministic maps, large values of η correspond to positive values of the Lyapunov exponent as we show below. For probabilistic processes, it is a measure of disorder. We define the normalized Boltzmann entropy η as

$$\eta = \frac{-1}{\log L} \sum_{i=1}^{L} q_i \log q_i, \quad (7)$$

where the interval $[0,1]$ is divided in L disjoint intervals I_i of equal size (bins) and q_i is the probability that $c \in I_i$, $i = 0,\ldots,L-1$. It is clear that $0 \leqslant \eta \leqslant 1$, the lower bound corresponding to a fixed point, the upper one to the uniform distribution $q_i = 1/L$. The probabilities q_i are found numerically by finding the fraction of time one orbit visits each of the subintervals I_i.

The map f of Eq. (5) depends on the parameters J, k, q, and ε. We keep q and ε fixed. By changing J for $k = 20$ we find the bifurcation diagram shown in Fig. 3(a) with the corresponding values of the Lyapunov exponent λ and the entropy η in Fig. 3(b). The bifurcation diagram appears to show a period-doubling cascade, but it is more complex than that. For $0 > J \geqslant J_0$ there are period-one orbits and for $J_0 > J \geqslant J_1$ period-two orbits. For $J_1 > J \geqslant J_2$ the orbits appear to have period four but actually correspond to two separate period-two attractors. In other words, there is a pitchfork bifurcation at $J = J_1$ For $J_2 > J \geqslant J_c$ there are two separate period-doubling bifurcations with the appearance of chaos at $J = J_c$. For $J_c > J \geqslant J_3$ there are two chaotic attractors that merge at $J = J_3$ [28]. Due to the symmetry of the map, Eq. (6), if c

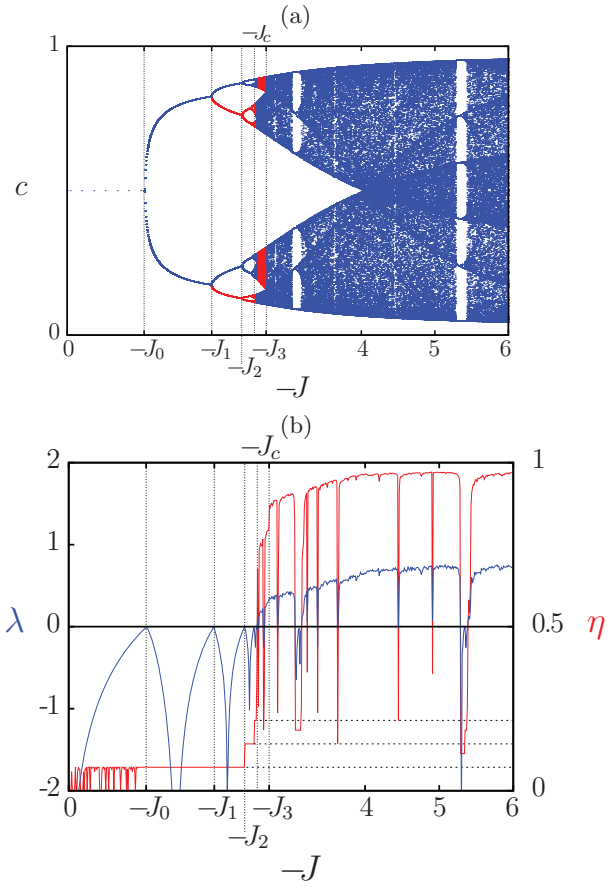

FIG. 3. (Color online) (a) Bifurcation diagram of the mean-field map, Eq. (5), by varying J. The doubling bifurcation route to chaos ends at $J = J_c$. For $0 > J \geqslant J_2$ and $J_3 > J \geqslant 6$ there is only one attractor (blue, darker dots). For $J_2 > J \geqslant J_c$ there are two: One of them corresponds to the lower branches that bifurcate up to J_c (red, lighter dots) and the other one to the upper branches (blue, darker dots). For $J_c > J \geqslant J_3$ there are two chaotic attractors, one corresponding to the lower branches (blue, darker dots) and the other to the top branches (red, lighter dots). For every value of J, the dots are 64 iterates of the map of Eq. (5) after a transient of 10^3 time steps. For values of J with only one basin of attraction the orbits do not depend on the initial average opinion $c(t = 0)$. For values of J that correspond to two attractors, one of them was found with $c(0) = 0.1$ and the other one with $c(0) = 0.9$. (b) The Lyapunov exponent λ [top curve on the left of the graph (in blue, darker)] and entropy η, [top curve on the right of the graph (in red, lighter)]. For every value of J, λ was evaluated during 10^3 time steps. The entropy η was computed using $L = 2^{14}$ bins. After a transient of 500 time steps, the probability distribution was evaluated during the next $100 \times L$ time steps. The horizontal dotted lines are drawn, starting from below, at $\eta = w/m$, $w = 1, \ldots, 3$ corresponding to periodic orbits of period 2^w. The connectivity is $k = 20$ and the vertical dotted lines are drawn at $J_0 = -1.045$, $J_1 = -1.965$, $J_2 = -2.375$, $J_c = -2.545$, and $J_3 = -2.705$.

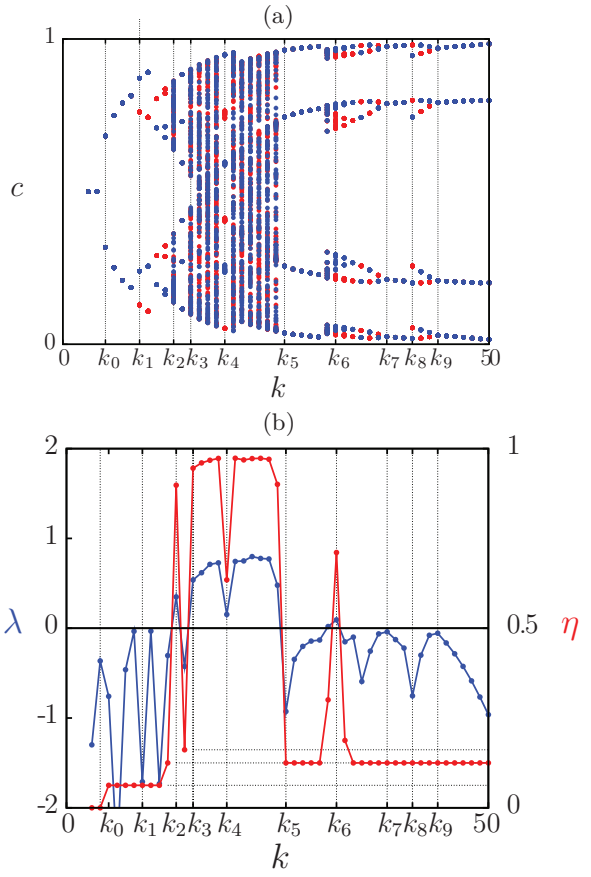

FIG. 4. (Color online) (a) Bifurcation diagram of the mean-field map of Eq. (5) varying k for $J = -6$. For every value of k, two initial values were considered, $c(0) = 0.1$ and $c(0) = 0.9$, and for each one 64 iterations were plotted after a transient of 10^3 time steps. For $k < k_0$ there is a fixed point and for $k_0 \leqslant k < k_1$ period-two orbits. For $k_1 \leqslant k < k_2$ the bottom branches (in red, lighter) correspond to one attractor and the top branches (in blue, darker) to the other one. For $k_3 \leqslant k < k_5$ the orbits are chaotic but for $k = k_4$ there are two attractors, one (in red) corresponds to the alternate clusters of points starting from below, the other one (in blue, darker) to the other three clusters of points. For $k_6 \leqslant k < k_7$, and $k_7 \leqslant k < k_8$ there are again two attractors, one cluster (in red, lighter) corresponds roughly to the bottom branches and the other one (in blue, darker) to the top branches. These attractors are not chaotic except for $k = k_6$. (b) The Lyapunov exponent λ, top curve for $k < k_2$ (in blue, darker), and the entropy η, top curve for $k_3 < k < k_5$ (in red, lighter), both as functions of the connectivity k for the same values of J as in (a). For each value of k, λ was evaluated during 10^3 time steps. For η, $L = 2^{16}$ and the probability distribution was evaluated during the $100 \times L$ time steps after a transient of 10^3 time steps. The horizontal dotted lines correspond, starting from below, to period-two, period-four, and period-six orbits. The vertical dotted lines are drawn at $k_0 = 5, k_1 = 9$, $k_2 = 13$, $k_3 = 15$, $k_4 = 19$, $k_5 = 26$, $k_6 = 32$, $k_7 = 38$, $k_8 = 41$, and $k_9 = 44$.

belongs to one of the basins of attraction, $1 - c$ belongs to the other one.

In Fig. 4(a) we show the bifurcation diagram of the map f as k changes with fixed J, ε, and q. For $k < k_0$ there are period-one orbits and for $k_0 \leqslant k < k_1$ period-two orbits. For $k_1 \leqslant k < k_2$ there are two period-two attractors. The two attractors are again present for $k = k_4$, $k_6 \leqslant k < k_7$, and $k_8 \leqslant k < k_9$. For $k = k_4$ and $k = k_6$ the two attractors are chaotic. In Fig. 4(b) we show λ and η as k changes. Again, chaotic orbits have entropy larger than $\eta_c = 1/2$. Chaotic orbits are present for $k = k_2$, $k_3 \leqslant k \leqslant k_5$, and $k = k_6$. Both bifurcation diagrams, Figs. 3(a)

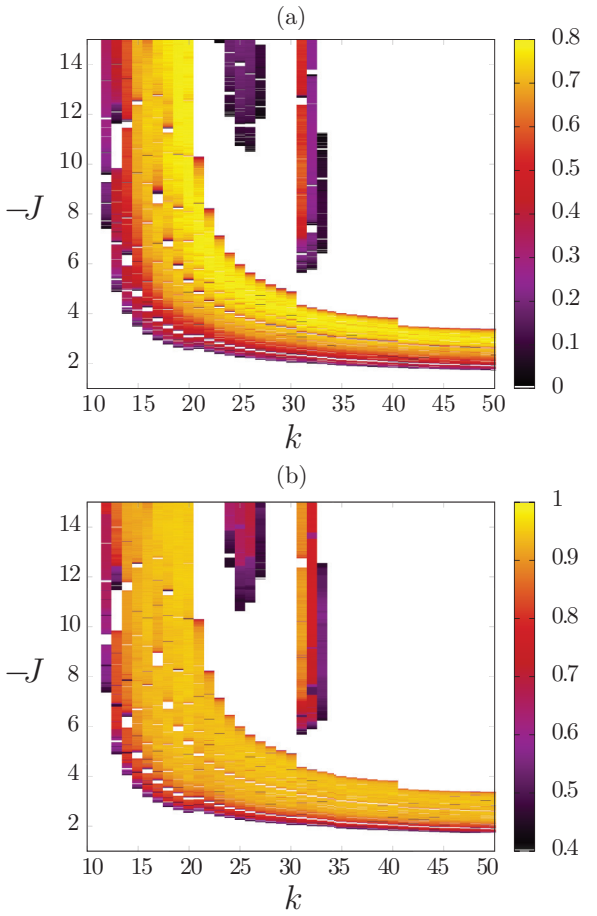

FIG. 5. (Color online) (a) Phase diagram showing positive values the Lyapunov exponent λ for the mean-field approximation [Eq. (5)] as a function of k and J. For each value of J and k the Lyapunov exponent λ was calculated during 10^3 time steps. (b) Phase diagram of the entropy η showing values larger than $1/2$ for the same values of ε and q as in (a). After a transient of $2 \cdot 10^3$ time steps the probability distribution was evaluated during the next 10^3 time steps on $L = 128$ bins.

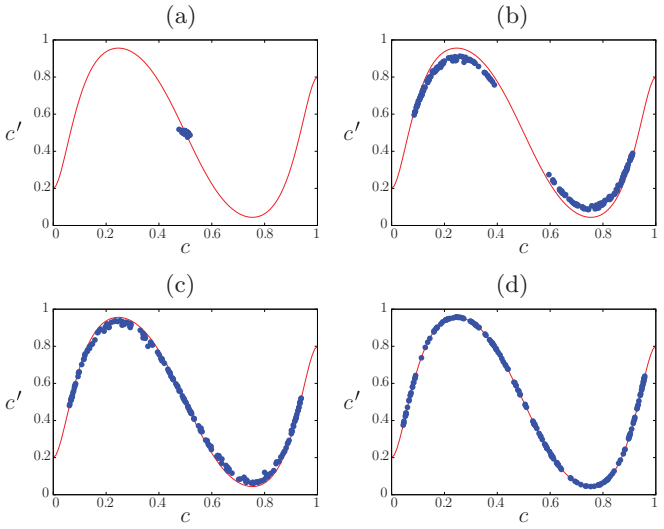

FIG. 6. (Color online) Return map of the average opinion c on small-world networks for several values of the long-range connection probability p with $J = -6$, $k = 20$, $N = 10^3$, and a transient of 10^3 time steps. The following 200 iterations are shown as (blue, darker) dots. The (red, lighter) continuous curve is Eq. (5). (a) $p = 0.0$, (b) $p = 0.5$, (c) $p = 0.6$, and (d) $p = 1.0$.

and 4(a), are symmetric around $c = 0.5$, a consequence of the symmetry of the mean-field map, Eq. (6).

In Figs. 5(a) and 5(b) we show the phase diagrams, as J and k change, of the Lyapunov exponent λ and the entropy η, respectively. In Fig. 5(a) the points correspond to $\lambda > 0$ and in Fig. 5(b) to $\eta > \eta_c = 1/2$. These figures show that both quantities are a good measure of chaos in this case. The values of λ and η shown in Fig. 3(b) correspond to those on a vertical line $k = 20$ of Figs. 5(a) and 5(b), respectively. The results shown in Fig. 4(b) correspond to a horizontal line $J = -6$ of Figs. 5(a) and 5(b). For $J < -15$ both phase diagrams show no qualitative change since the transition probability $\tau(h)$ is essentially a step function.

IV. SMALL-WORLD NETWORKS

In the Watts-Strogatz small-world network model there is a smooth change from a regular to a random lattice [11]. Starting with a network with N agents, where the neighborhood of each agent is formed by his k nearest neighbors, with probability p each neighbor is replaced by another agent chosen at random among those that are not in the neighborhood. We call p the long-range connection probability. In Fig. 6 we show the return map of the average opinion c, after a long transient, together with the mean-field return map f of Eq. (5) for several values of p. For $p = 0$, the density c fluctuates around its mean value 0.5. As p grows, the system becomes more homogeneous and the distribution of points approaches the mean-field behavior, even though the mean-field approximation is based on the absence of correlations. As shown in the figure, for $p = 0.6$ the return map is already close to the mean-field behavior and for $p = 1$ it is indistinguishable from it.

We show in Figs. 7(a) and 7(b) the probabilistic bifurcation diagrams of c as a function of the probability of long-range connections p for $J = -6$ and $J = -3$ and the same value of k. In both figures, for $0 < p \lesssim p_0$ and $p_0 < p \lesssim p_1$ we can identify period-one and period-two orbits, respectively. For $p_1 \lesssim p \lesssim p_2$ there are two period-two attractors which become indistinguishable for $p \simeq p_2$. For $p_2 \lesssim p$ there is only one attractor. In Figs. 7(b) and 7(c) we show the corresponding entropy. We would like to find a threshold η_d for the appearance of disorder, similar to η_c of the mean-field approximation, and we propose $\eta_d = \eta(p_2)$ shown as the horizontal lines in Figs. 7.

In Figs. 8(a) and 8(b) we show the phase diagrams of the entropy η for $p = 0.5$ and $p = 1$, respectively. It is evident that for $p = 1$ [Fig. 8(b)] the diagram is very similar to that of Fig. 5(b), while for $p = 0.5$ [Fig. 8(a)] the region where $\eta > \eta_d$ extends to larger values of k. The dependence on J is much less marked. It is possible to roughly understand these results assuming that the main contributions to the mean-field character of the collective behavior come from the fraction of links that are rewired (long-range connections) and that depend on p.

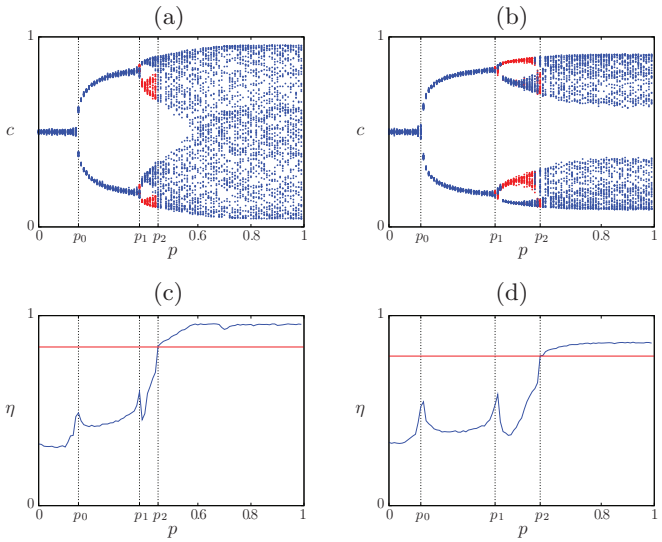

FIG. 7. (Color online) [(a) and (b)] Small-world probabilistic bifurcation diagrams as functions of the long-range probability p. For $p \lesssim p_0$ there are almost periodic orbits of period one and for $p_0 \lesssim p \lesssim p_1$ of period two. For $p_1 \lesssim p \lesssim p_2$ we find two attractors, one (in red, lighter) in the lower branches and the other one (in blue, darker) in the top ones. [(c) and (d)] The entropy η as a function of p. The (red, lighter) lines mark the value of η_d. [(a) and (c)] $J = -6$, $p_0 \sim 0.15$, $p_1 \sim 0.38$, $p_2 \sim 0.45$, and $\eta_d = \eta(p_2) = 0.835$. [(b) and (d)] $J = -3$, $p_0 \sim 0.12$, $p_1 \sim 0.40$, $p_2 \sim 0.57$, and $\eta_d = \eta(p_2) = 0.787$. In (a) and (b) the number of agents is $N = 5 \times 10^4$, the connectivity is $k = 20$. After a transient of 4×10^3 time steps, the probability distribution is evaluated using $L = 256$ bins during the next $100 \times L$ time steps.

V. SCALE-FREE NETWORKS

Human and technological networks often present a scale-free character, with different degrees of correlation among nodes. In this section we present results of the model on uncorrelated scale-free networks [12]. Starting from a fully connected group of m agents, other $N - m$ agents join sequentially, each one choosing m neighbors among those already in the group. The choice is preferential; the probability that a new member chooses agent i is proportional to its connectivity k_i, the number of neighbors agent i already has. Another way of building the network is to choose a random edge of a random node and connect to the other end of the edge, since such an edge arrives to a vertex with probability proportional to $kp(k)$ [29].

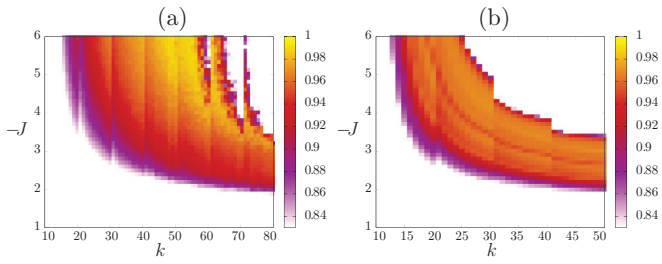

FIG. 8. (Color online) Entropy phase diagrams of simulations on small-world networks as functions of k and J for (a) $p = 0.5$ and (b) $p = 1.0$. The colored region corresponds to $\eta > \eta_d = 0.8$. Entropy computed with 128 bins, lattice size $N = 10^4$, sampling time 1.2×10^4 steps after a transient of 4×10^3 steps.

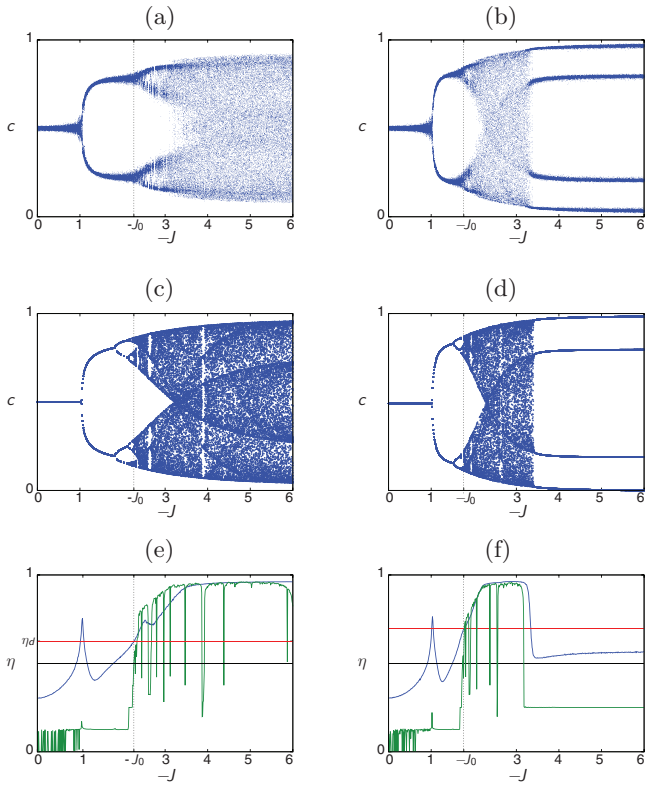

FIG. 9. (Color online) Comparisons between simulations on scale-free networks and mean-field approximation. In (a) and (b) bifurcation diagrams of simulations on scale-free networks with $m = 15$ and $m = 30$, respectively. In both cases, the number of agents is $N = 10\,000$ and for every value of J, the initial opinions are chosen at random with $c = 1/2$, and 128 values of c are plotted after a transient of 300 time steps. In (c) and (d) we show the bifurcation diagrams of the mean-field approximation with $k = 25 \sim 1.7 \times 15$ and $k = 51 \sim 1.7 \times 30$, respectively. In both figures, $c(0)$ is chosen at random and 128 values of c are plotted after a transient of 10^3 time steps. In (e) and (f) the entropy η of the simulations on scale-free networks [top curve (blue) for $J > -1$] is compared with that of the mean-field approximation [bottom curve (green) for $J > -1$]. In (e), $k = 15$ and $m = 25$, in (f) $k = 30$ and $m = 51$. The entropy is found by dividing the unit interval in 256 bins. For each value of J, $c(0) = 0.1$ and after a transient of 10^3 time steps the entropy was evaluated during the following 2.56×10^4 time steps. In (a) and (e) $J_0 = -2.267$, and in (b) and (f) $J_0 = -1.766$.

In the appendix we show that the model dynamics on scale-free networks is comparable to the mean-field approximation of Sec. III on a network with constant connectivity k with

$$k = \alpha m, \qquad \alpha \sim 1.7. \tag{8}$$

In Figs. 9(a) and 9(b) we show the probabilistic bifurcation diagrams of the model on scale-free networks as a function of J for two values of m and in Figs. 9(c) and 9(d) we show the bifurcation diagram of the mean-field approximation [Eq. (5)] for the corresponding values of k according to Eq. (8). We find a qualitative agreement between these bifurcation diagrams.

In Figs. 9(e) and 9(f) we show the entropy of of the mean-field approximation and of the simulations on scale-free networks. We find a reasonable agreement when $\eta > \eta_d$ with $\eta_d = \eta(J_0)$ and J_0 the value of J for which the entropy of the mean-field approximation crosses the line $\eta = 1/2$ for the first time. Thus, the entropy is a good way of comparing both dynamics when k and m are related according to Eq. (8). Above η_d, both entropies are numerically similar, except where there are periodic windows in the mean-field approximation, and this agreement is better for $m = 30$ and $k = 51$.

VI. CONCLUSIONS

We studied a reasonable contrarian opinion model. The reasonableness condition forbids the presence of absorbing states. In the model, this condition depends on two parameters that are held fixed. The model also depends on the connectivity k which may vary among agents, and the coupling parameter J. The neighborhood of each agent is defined by an adjacency matrix that can have fixed or variable connectivity (fixed or power law) and a regular or stochastic character. The interesting observable is the average opinion c at time t. We computed the entropy η of the stationary distribution of c, after a transient.

In the simplest case, the neighborhood of each agent includes k random sites. In this case, the mean-field approximation for the time evolution of the average opinion exhibits, by changing J, a period doubling bifurcation cascade towards chaos with an interspaced pitchfork bifurcation. A positive (negative) Lyapunov exponent corresponds to an entropy larger (smaller) than $\eta_c = 1/2$. Thus, entropy is a good measure of chaos for this map and can be also used in the simulations of the stochastic microscopic model.

The bifurcation diagram of the mean-field approximation as a function of k shows periodic and chaotic regions, also with a pitchfork bifurcation. Again, entropies larger than η_c correspond to chaotic orbits.

Actual simulations on a one-dimensional lattice show incoherent local oscillations around $c = 1/2$. By rewiring at random a fraction p of local connections, the model presents a series of bifurcations induced by the small-world effect: The density c exhibits a probabilistic bifurcation diagram that resembles that obtained by varying J in the mean-field approximation. These small-world induced bifurcations are consistent with the general trend whereby long-range connections induce mean-field behavior. This is the first observation of this for a system exhibiting a *chaotic* mean-field behavior. Indeed, the small-world effect makes the system more coherent (with varying degree). We think that this observation may be useful since many theoretical studies of population behavior have been based on mean-field assumptions (differential equations), while actually one should rather consider agents, and therefore spatially extended, microscopic simulations. The well-stirred assumption is often not sustainable from the experimental point of view. However, it may well be that there is a small fraction of long-range interactions (or jumps) that might justify the small-world effect.

The model on scale-free networks with a minimum connectivity m shows a similar behavior to that of the mean-field approximation of the model on a network with constant connectivity k [Eq. (5)] if $k = \alpha m$ with $\alpha \sim 1.7$.

In summary, we have found that, as usual, long-range rewiring leads to mean-field behavior, which can become chaotic by varying the coupling or the connectivity. Similar scenarios are found in actual microscopic simulations, also by varying the long-range connectivity, and in scale-free networks.

The model can be extended to cases where there are both contrarians and conformists, where the neighborhoods change in time and even where the political mood (contrarian or conformist) can change according to the social pressure (local field). Any one of these extensions can lead to interesting behavior. This study can have applications to the investigation of collective phenomena in algorithmic trading.

ACKNOWLEDGMENTS

Interesting discussions with Jorge Carneiro and Ricardo Lima are acknowledged. This work was partially supported by Recognition Project UE Grant No. 257756 and project PAPIIT-DGAPA-UNAM IN109213.

APPENDIX

The similarity between the bifurcations diagrams in Figs. 3(a) and 4(a), which comes from the similarities of the mean-field maps when changing J and k (Fig. 2), can be explained by using a continuous approximation for the connectivity k. By using Stirling's approximation for the binomial coefficients in Eq. (5), for intermediate values of c [30], we obtain

$$\binom{k}{w} c^w (1-c)^{k-w} \simeq \frac{1}{\sqrt{2\pi k c(1-c)}} \exp\left[\frac{-k\,(w/k-c)^2}{2c(1-c)}\right]. \tag{A1}$$

In this approximation, Eq. (5) can be written as

$$c' = \int_{-\infty}^{\infty} dx \sqrt{\frac{k}{2\pi c(1-c)}} \exp\left[-\frac{k(x-c)^2}{2c(1-c)}\right] \tau(x), \tag{A2}$$

with x the continuous approximation of w/k. This expression is just a Gaussian convolution of τ, i.e., a smoothing of the transition probability, as can be seen by comparing Fig. 1 with Fig. 2. This smoothing has the effect of reducing the slope of the curve in a way similar to changing J (but it depends also on c), and this explains the similarities between the bifurcation diagrams in Figs. 3(a) and 4(a). For instance, Fig. 3(a) is obtained for $k = 20$, a value that in Fig. 4(a) corresponds to a chaotic strip just after a window with six branches. A similar window can be observed also in Fig. 3(a) by increasing J from the value $J = -6$ of Fig. 4(a).

This approximation can be used also to find the "effective" connectivity of the model on a scale-free network. The mean-field approximation for a nonhomogeneous network can be written as

$$c'_k = \sum_{\substack{s_1,s_2,\ldots,s_k \\ j_1,j_2,\ldots,j_k}} \prod_{i=1}^{k} c_{j_i}^{s_i} (1-c_{j_i})^{1-s_i} Q(j_i|k) \tau(h_i), \tag{A3}$$

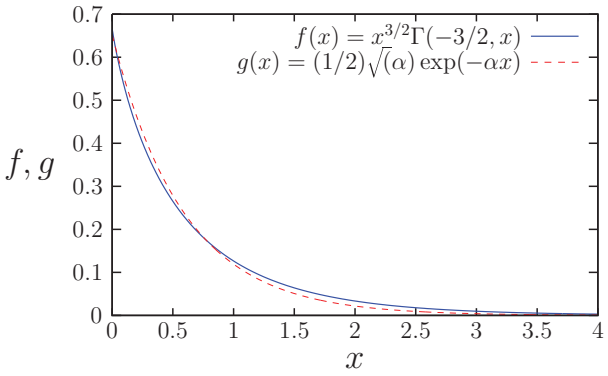

FIG. 10. (Color online) Comparisons between the two functions $f(x)$ (blue, solid line) and $g(x)$ (red, dashed line), for $\alpha = 1.7$, corresponding to the minimum of $\int_0^4 (f(x) - g(x))^2 dx$.

with c'_k the probability that the opinion of an agent with connectivity k at time $t+1$ is 1, and c_j the probability that the opinion of an agent with connectivity j at time t is 1. The sum on the right-hand side is taken over the opinions $s_1, \ldots, s_k$ of the k agents in the neighborhood and over their connectivities $j_1, \ldots, j_k$. The variables s_i take the values zero or 1, while j_i ranges from m to ∞. The quantity $Q(j|k)$ is the probability that the agent with connectivity j is connected to another one of connectivity k and $\sum_j Q(j|k) = 1$.

Since this network is symmetric, $kQ(j|k)P(k) = jQ(k|j)P(j)$ (detailed balance). It is also nonassortative, so $Q(j|k)$ does not depend on k and we can write $Q(j|k) = \phi(j)$. By summing the detailed balance condition over j we get $\phi(k) = kP(k)/\langle k\rangle$.

Therefore, Eq. (A3) becomes

$$c'_k = \sum_{s_1, s_2, \ldots, s_k} \tau\left(\frac{\sum_i s_i}{k}\right) \prod_{i=1}^{k} \sum_{j_i} \frac{j_i P(j_i)}{\langle k\rangle} c_{j_i}^{s_i} (1 - c_{j_i})^{1-s_i}. \tag{A4}$$

In the previous equation, s_i is either zero or 1, so only one between $c_{j_i}^{s_i}$ and $(1 - c_{j_i})^{1-s_i}$ differs from zero. Assuming that c_k depends only slightly on k in Eq. (A4), we approximate $(\sum_{j_i} j_i P(j_i) c_{j_i})/\langle k\rangle$ with c and we get

$$\begin{aligned} c'_k &= \sum_{s_1, s_2, \ldots, s_k} \tau\left(\frac{\sum_i s_i}{k}\right) \prod_{i=1}^{k} c^{s_i} (1-c)^{1-s_i}, \\ &= \sum_w \tau\left(\frac{w}{k}\right) \binom{k}{w} c^w (1-c)^{k-w}, \end{aligned}$$

with $w = \sum_i s_i$. In order to close the equation, we average c'_k over the probability distribution $P(k)$.

By using the approximation of Eq. (A1), we get

$$\begin{aligned} c' &= \sum_{k=m}^{\infty} P(k) \sum_w \tau\left(\frac{w}{k}\right) \binom{k}{w} c^w (1-c)^{k-w} \\ &\simeq \int_m^{\infty} dk\ P(k) \int_{-\infty}^{\infty} dx\ \tau(x) \sqrt{\frac{k}{2\pi c(1-c)}} \\ &\quad \times \exp\left[-\frac{k(x-c)^2}{2c(1-c)}\right], \end{aligned}$$

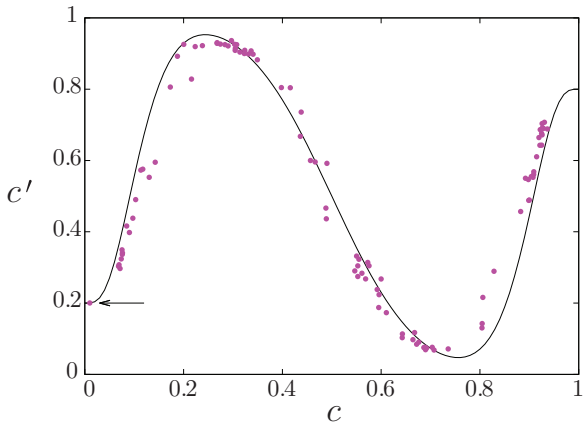

FIG. 11. (Color online) First 100 steps of the return map for the density c of the model on a scale-free network with $N = 10^4$, $m = 20$, $J = -4$. The first iterate is marked by the arrow. The continuous curve is the graph of Eq. (A5) with $k = 34$.

where $x = w/k$. For scale-free networks the connectivity distribution P is given by $P(k) = 2m^2 k^{-3}$. Then

$$\begin{aligned} c' &\simeq \int_{-\infty}^{\infty} dx \frac{2m^2 \tau(x)}{\sqrt{(2\pi c(1-c))}} \int_m^{\infty} dk\ k^{-5/2} \exp(-kA), \\ &= \int_{-\infty}^{\infty} dx \frac{m^{1/2}\tau(x)}{(2\pi c(1-c))^{1/2}} 2(mA)^{3/2} \Gamma\left(-\frac{3}{2}, mA\right), \end{aligned}$$

where $A = A(x) = (x-c)^2/(2c(1-c))$ and $\Gamma(a,x)$ is the incomplete upper gamma function extended to negative values of a (the function $x^{-a}\Gamma(a,x)$ is single-valued and analytic for all values of a and x [31]).

The function $f(y) = y^{3/2}\Gamma(-3/2, y)$ is well approximated by $g(y) = (1/2)\sqrt{\alpha}\exp(-\alpha y)$, as shown in Fig. 10. Therefore we can write

$$c' \simeq \int_{-\infty}^{\infty} dx\ \tau(x) \sqrt{\frac{\alpha m}{2\pi c(1-c)}} \exp\left[-\frac{\alpha m (x-c)^2}{2c(1-c)}\right].$$

This last expression has the form of Eq. (A2), with an effective connectivity $\tilde{k} = \alpha m$.

Since the argument y of $g(y)$ is $mA(x) = m(x-c)^2/(2c(1-c))$, the substituted $g(x)$ results to be a Gaussian, centered around $x = c$. The important values of $g(x)$ lie between 0 and 4, depending on the value of c. In this interval, the best approximation of $f(y)$ (the minimum of $\int_0^4 (f(y) - g(y)^2 dy$) is around $\alpha \simeq 1.7$. Therefore $\tilde{k}$ definitively differs from the average connectivity $\langle k\rangle = 2m$.

In conclusion, as in the case of a nonassortative scale-free network, the probability of getting a site with value 1 in the mean-field approximation is given by

$$c' = \sum_{j=0}^{\tilde{k}} c^j\ (1-c)^{\tilde{k}-j}\ \tau\left(\frac{j}{\tilde{k}}\right), \tag{A5}$$

with $\tilde{k} \simeq 1.7m$.

As usual, the mean-field predictions are only approximately followed by actual simulations. In Fig. 11 we show the first 100 steps of the return map of the density c for $J = -0.4$. The scale-free network is fixed, with $m = 20$, $N = 10\,000$

and the initial opinions of the agents are chosen at random with $c = 0.01$. The arrow marks the first point that follows the mean-field prediction with $\alpha = 1.7$ ($\tilde{k} = 34$), as in Fig. 11, but then, due to correlations, the return maps follows a different curve. This implies that nontrivial correlations establish also in scale-free networks.

[1] J. Binney, N. Dowrick, A. Fisher, and M. Newman, *The Theory of Critical Phenomena: An Introduction to the Renormalization Group* (Oxford University Press, Oxford, 1992).

[2] R. N. Costa Filho, M. P. Almeida, J. S. Andrade Jr., and J. E. Moreira, Phys. Rev. E **60**, 1067 (1999); M. C. Mantovani, H. V. Ribeiro, M. V. Moro, and R. S. Mendes, Europhys. Lett. **96**, 48001 (2011); A. Chatterjee, M. Mitrović, and S. Fortunato, Sci. Rep. **3**, 1049 (2013).

[3] S. N. Dorogovtsev and J. F. F. Mendes, *Evolution of Networks: From Biological Nets to the Internet and WWW* (Oxford University Press, Oxford, 2005).

[4] C. Castellano, S. Fortunato, and V. Loreto, Rev. Mod. Phys. **81**, 591 (2009).

[5] R. Axelrod, *The Evolution of Cooperation* (Basic Books, New York, 1984); M. A. Nowak, *Evolutionary Dynamics: Exploring the Equations of Life* (Belknap Press, Boston, 2006).

[6] D. Stauffer, AIP Conf. Proc. **779**, 56 (2005); S. Galam, Int. J. Mod. Phys. C **19**, 409 (2008); *Sociophysics: A Physicist's Modeling of Psycho-Political Phenomena* (Springer, Berlin, 2012).

[7] G. Deffuant, Adv. Compl. Sys. **3**, 87 (2000).

[8] A. Corcos, J.-P. Eckmann, A. Malaspinas, Y. Malevergne, and D. Sornette, Quant. Financ. **2**, 264 (2002).

[9] S. Galam, Physica A **333**, 453 (2004).

[10] S. Biswas, A. Chatterjee, and P. Sen, Physica A **391**, 3257 (2012).

[11] D. J. Watts and S. H. Strogatz, Nature **393**, 440 (1998).

[12] L. Barabási and R. Albert, Science **286**, 509 (1999).

[13] K. Klemm, V. M. Eguiluz, R. Toral, and M. San Miguel, Phys. Rev. E **67**, 026120 (2003).

[14] B. Wu, D. Zhou, and L. Wang, Phys. Rev. E **84**, 046111 (2011).

[15] P. Holme and M. E. J. Newman, Phys. Rev. E **74**, 056108 (2006).

[16] M. A. Nowak, Science **314**, 1560 (2006); C. Taylor and M. A. Nowak, Evolution **61**, 2281 (2007).

[17] B. Wu, P. M. Altrock, L. Wang, and A. Traulsen, Phys. Rev. E **82**, 046106 (2010).

[18] A. Traulsen, M. A. Nowak, and J. M. Pacheco, Phys. Rev. E **74**, 011909 (2006).

[19] W. Brian Arthur, Am. Econ. Rev. **84**, 406 (1994); D. Challet and Y.-C. Zhang, Physica A **246**, 407 (1997).

[20] P. Jain, J. Financ. **60**, 2955 (2005).

[21] A. Chaboud, B. Chiquoine, E. Hjalmarsson, and C. Vega (unpublished).

[22] F. Bagnoli, F. Franci, and R. Rechtman, in *Cellular Automata*, edited by S. Bandini, B. Chopard, and M. Tomassini (Springer-Verlag, Berlin, 2002), p. 249.

[23] F. Bagnoli, F. Franci, and R. Rechtman, Phys. Rev. E **71**, 046108 (2005).

[24] B. Derrida, in *Fundamental Problems in Statistical Mechanics*, edited by H. van Beijeren (Elsevier, New York, 1990), Vol. VII., p. 276.

[25] F. Bagnoli, N. Boccara, and R. Rechtman, Phys. Rev. E **63**, 046116 (2001).

[26] A. Ilachinski, *Cellular Automata: A Discrete Universe* (World Scientific, Singapore, 2001), p. 352.

[27] L. Boltzmann, *Vorlesungen über Gastheorie* (J. A. Barth, Leipzig, 1896 and 1898) [English translation by S. G. Brush, *Lectures on Gas Theory* (University of California Press, Los Angeles, 1964), Chap. I, Sec. 6.].

[28] H. E. Nusse and J. A. Yorke, Physica D **57**, 39 (1992); H. E. Nusse, E. Ott, and J. A. Yorke, Phys. Rev. E **49**, 1073 (1994); V. Avrutin, M. Schanz, *ibid.* **70**, 026222 (2004).

[29] M. E. J. Newman, S. H. Strogatz, and D. J. Watts, Phys. Rev. E **64**, 026118 (2001).

[30] E. Ott, *Chaos in Dynamical Systems* (Cambridge University Press, Cambridge, 2002).

[31] M. Abramowitz and I. Stegun, *Handbook of Mathematical Functions* (Dover, New York, 1985), pp. 260–261.